journal of the mechanical behavior of biomedical materials 157 (2024) 106634

Contents lists available at ScienceDirect

Journal of the Mechanical Behavior of Biomedical Materials

journal homepage: www.elsevier.com/locate/jmbbm

Comparison of simplified bone-screw interface models in materially nonlinear μFE simulations

Pia Stefanek [a,*], Dieter H. Pahr [a,b], Alexander Synek [a]

[a] Institute of Lightweight Design and Structural Biomechanics, TU Wien, Austria
[b] Division Biomechanics, Karl Landsteiner University of Health Sciences, Austria

ARTICLE INFO

Keywords:
Micro finite element modelling
Materially-nonlinear explicit simulation
Bone-screw system
Bone-screw interface modelling

ABSTRACT

Micro finite-element (μFE) simulations serve as a crucial research tool to assist laboratory experiments in the biomechanical assessment of screw anchorage in bone. However, accurately modelling the interface between bone and screw threads at the microscale poses a significant challenge. Currently, the gold-standard approach involves employing computationally intensive physical contact models to simulate this interface. This study compared nonlinear μFE predictions of deformations, whole-construct stiffness, maximum force and damage patterns of three different computationally efficient simplified interface approaches to the general contact interface in Abaqus Explicit, which was defined as gold-standard and reference model. The μCT images (resolution: 32.8 μm) of two human radii with varying bone volume fractions were utilized and a screw was virtually inserted up to 50% and 100% of the volar-dorsal cortex distance. Materially nonlinear μFE models were generated and loaded in tension, compression and shear. In a first step, the common simplification of using a fully-bonded interface was compared to the general contact interface, revealing overestimations of whole-construct stiffness (19% on average) and maximum force (26% on average), along with inaccurate damage pattern replications. To enhance predictions, two additional simplified interface models were compared: tensionally strained element deletion (TED) and a novel modification of TED (TED-M). TED deletes interface elements strained in tension based on a linear-elastic simulation before the actual simulation. TED-M extends the remaining contact interface of TED by incorporating neighboring elements to the contact area. Both TED and TED-M reduced the errors in whole-construct stiffness and maximum force and improved the replication of the damage distributions in comparison to the fully-bonded approach. TED was better in predicting whole-construct stiffness (average error of 1%), while TED-M showed lowest errors in maximum force (1% on average). In conclusion, both TED and TED-M offer computationally efficient alternatives to physical contact modelling, although the fully-bonded interface may deliver sufficiently accurate predictions for many applications.

1. Introduction

For more than five decades finite element (FE) simulations have served as invaluable tools in bone implant development and evaluation, complementing laboratory experiments (Taylor and Prendergast, 2015). Unlike laboratory experiments, numerical studies are cost- and time-effective and do not rely on tissue samples which can be difficult to obtain. Micro-finite element (μFE) simulations, based on high-resolution computed tomography (CT) scans, currently represent the gold standard, particularly for the challenging task of modelling screw anchorage in trabecular bone. They are able to resolve the bone-screw interface on the microscale and hence capture the screw thread geometry as well as peri-implant bone region in detail, which was reported to be essential for an accurate prediction of the mechanical behavior of the bone-screw system (Marcián et al., 2021; Wirth et al., 2011, 2012).

Bone-screw μFE simulations have to overcome two major challenges: bone-screw interface modelling and simulation of pre-damage due to screw insertion. Usually, linear-elastic μFE simulation studies assumed a fully-bonded interface and neglected pre-damage in the peri-implant bone region. They reported overestimations in whole-construct stiffness and strains up to one order of magnitude (Steiner et al., 2017; Torcasio et al., 2012; Wirth et al., 2010). In order to account for the reduction in mechanical competence of the peri-implant bone region (Lee and Baek, 2010; Steiner et al., 2016; Wang et al., 2012), Steiner

* Corresponding author. Gumpendorfer Straße 7, A-1060, Wien, Austria.
E-mail address: stefanek@ilsb.tuwien.ac.at (P. Stefanek).

https://doi.org/10.1016/j.jmbbm.2024.106634
Received 11 April 2024; Received in revised form 3 June 2024; Accepted 18 June 2024
Available online 21 June 2024

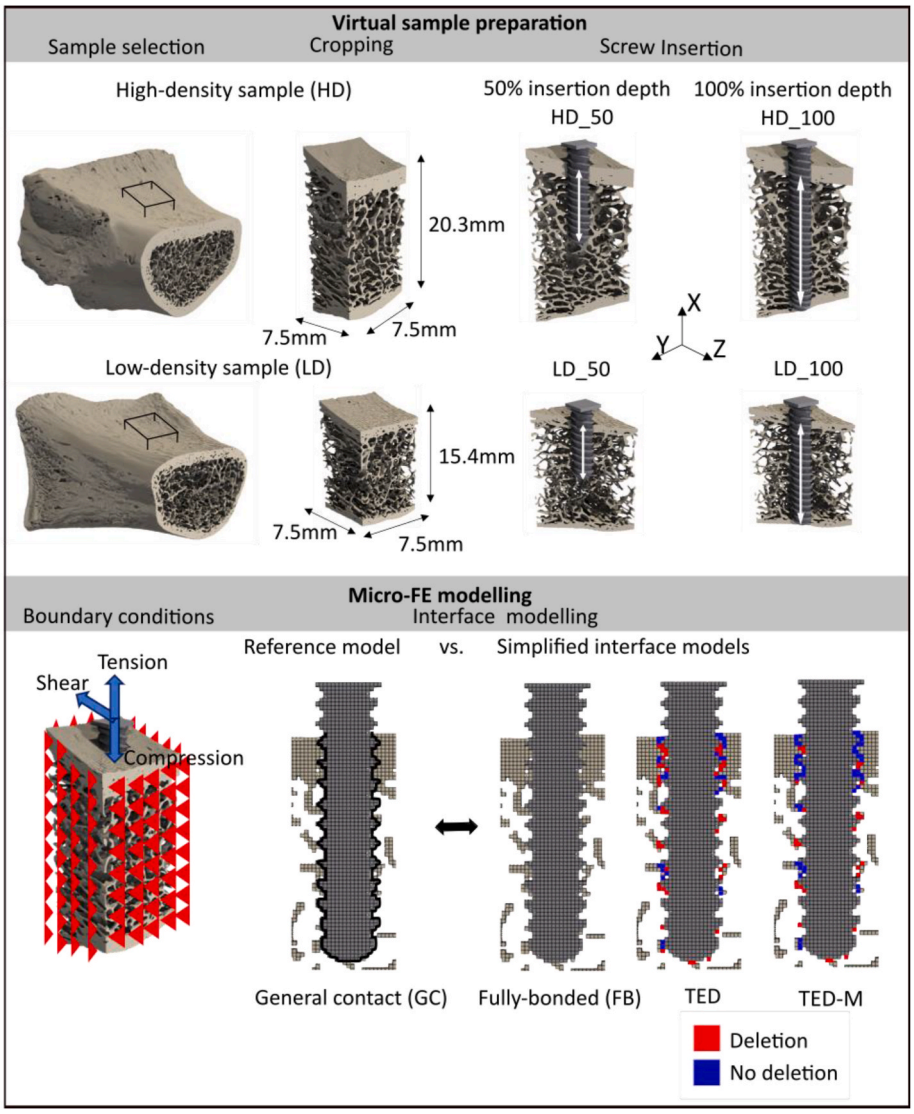

Fig. 1. Outline of the study. This figure shows the interface models with lower resolution in order to schematically illustrate the differences at the interface.

et al. (2017) and Torcasio et al. (2012) implemented a peri-implant damage zone with reduced stiffness in their linear-elastic μFE simulations and were able to reduce the errors in the predicted strain and whole-construct stiffness to about 10% on average. Since the bone-screw failure process as well as the contact mechanics at the bone-screw interface are highly nonlinear, recent studies have turned to nonlinear μFE simulations. Most of them included frictional contact at the bone-screw interface but ignored peri-implant bone damage (Ovesy et al., 2022; Panagiotopoulou et al., 2021). Nevertheless, they were able to improve the predictions in comparison to the linear-elastic simulations and were able to quantitatively replicate the experimentally measured screw perforation force (Panagiotopoulou et al., 2021) and screw pull-out force (Ovesy et al., 2022).

Nonlinear μFE models are typically solved with general-purpose FE solvers (e.g. Abaqus, Dassault Systems, Vélizy-Villacoublay, France) which can handle different types of nonlinearities (geometric, material and contact) but are computationally demanding. Ovesy et al. (2022) reported solving times of 2h on 16 cores for relatively small models, consisting of a single screw with an average model size of 350,000 elements. In consequence, many nonlinear studies needed to reduce the model sizes by either cropping the bone specimens (Ovesy et al., 2022) or decreasing the image resolution (Panagiotopoulou et al., 2021) in order to achieve manageable solving times. The capability to simulate a complete bone-screw implant system, including multiple screws, can only be achieved using specialized solvers designed to solve large-scale problems (e.g. FEAP, Taylor, 2014), Faim (Numerics88 Solutions Ltd, https://bonelab.github.io/n88/index.html), ParOSol (Flaig and Arbenz, 2012), ParOSol-NL (Stipsitz et al., 2020)). These solvers exhibit improved parallel execution performance and can handle nonlinear models with several hundreds of million elements (Stipsitz and Pahr, 2018). However, the application of these efficient solvers always comes with the drawback of reduced model complexity, as they typically only incorporate linear-elastic or simple nonlinear material laws and lack bone-screw contact implementations. To address these limitations, some researchers employed simplified interface model approaches that try to avoid the occurrence of artificial tensile strain on the interface elements. For example, Ovesy et al. (2022) and Panagiotopoulou et al. (2021), removed the bone elements directly below the screw threads specifically for simulated screw pull-out loading cases. Steiner et al. (2017) developed a method independent of the loading case: they conducted an initial linear simulation that was used to calculate the volumetric strain of the interface elements. Then they removed all interface elements undergoing positive volumetric strain and performed the simulation with the updated interface again.

Despite these efforts, the necessity of including contact at the bone-screw interface in μFE models is still in question. The available literature

Table 1
Dimensions and CT-based morphometrics of the two prepared bone specimens.

Specimen	Side length in mm	Height in mm	Trabecular bone			Cortical bone
			BV/TV in %	Tb.Th[a] in µm	Tb.Sp[a] in µm	C.Th[a] in µm
LD	7.5	14.5	12.5	194 ± 56	939 ± 315	494 ± 135
HD	7.5	20.3	21.4	228 ± 66	811 ± 247	690 ± 234

Note: bone volume fraction (BV/TV), trabecular thickness (Tb.Th), trabecular separation (Tb.Sp), volar and dorsal cortical thickness (C.Th), low-density specimen (LD), high-density specimen (HD).
[a] Mean ± standard deviation.

on this subject matter is limited as the effects of interface modelling and peri-implant bone damage due to screw insertion overlap and its influences cannot be discriminated in lab experiments. One of the few studies on this topic was conducted by Steiner et al. (2017). They only found minimal whole-construct stiffness differences when comparing the fully-bonded interface to a simplified interface model approach using linear-elastic µFE models. To the authors' knowledge no study yet examined the relevance of interface modelling in the nonlinear regime.

The first aim of this study was to investigate the influence of physical contact modelling regarding deformations, whole-construct stiffness, maximum force and damage distribution using nonlinear µFE in Abaqus Explicit. In a second step, the performance of the already existing simplified interface model of Steiner et al. (2017) was evaluated and compared to a newly developed interface model that was found based on a qualitative and quantitative analysis of the contact area. In order to concentrate on the effects of interface modelling in an isolated manner, damage due to screw-insertion was excluded. As this cannot be done experimentally, this study was conducted solely numerical using general contact in Abaqus Explicit as gold-standard and reference model. The study design enables direct transfer of the simplified interface models to highly efficient µFE solvers such as ParOSol-NL.

2. Material and methods

Fig. 1 shows the outline of this study. All details can be found below. Shortly, two human radius bone specimens with low and high bone densities were cropped and a screw was virtually inserted. Voxel-based nonlinear µFE models were generated, and three loading cases (tension, compression, and shear) were simulated using Abaqus Explicit. Deformations, whole-construct stiffness, maximum force, and damage distribution within the bone were evaluated. Three different simplified interface models (fully-bonded and "element deletion" models) were compared to a reference model (general contact).

2.1. Image processing

Micro-computed tomography (µCT) images of human distal radius sections from previous studies (Hosseini et al., 2017; Synek et al., 2023) were used (see Fig. 1). The original scans had a resolution of 16.4 µm and were taken by Hosseini et al. (2017) using a µCT 100 scanner (SCANCO Medical AG, Brüttisellen, Switzerland). Stipsitz et al. (2021) segmented and resampled the images to a resolution of 32.8 µm. This resolution was chosen to ensure applicability of the material model of Stipsitz et al. (2020) (see section 2.2) which was developed for resolutions around 35 µm. From 15 specimens in total, two specimens that differed in their bone volume fraction were selected: a low-density (LD) and high-density specimen (HD). The images were uniformly aligned with respect to the volar surface and a cuboid with a square cross section of 7.5 mm side length was cropped from the center of the bones (see Table 1). The cuboid size was selected according to Ovesy et al. (2019, 2022) with the

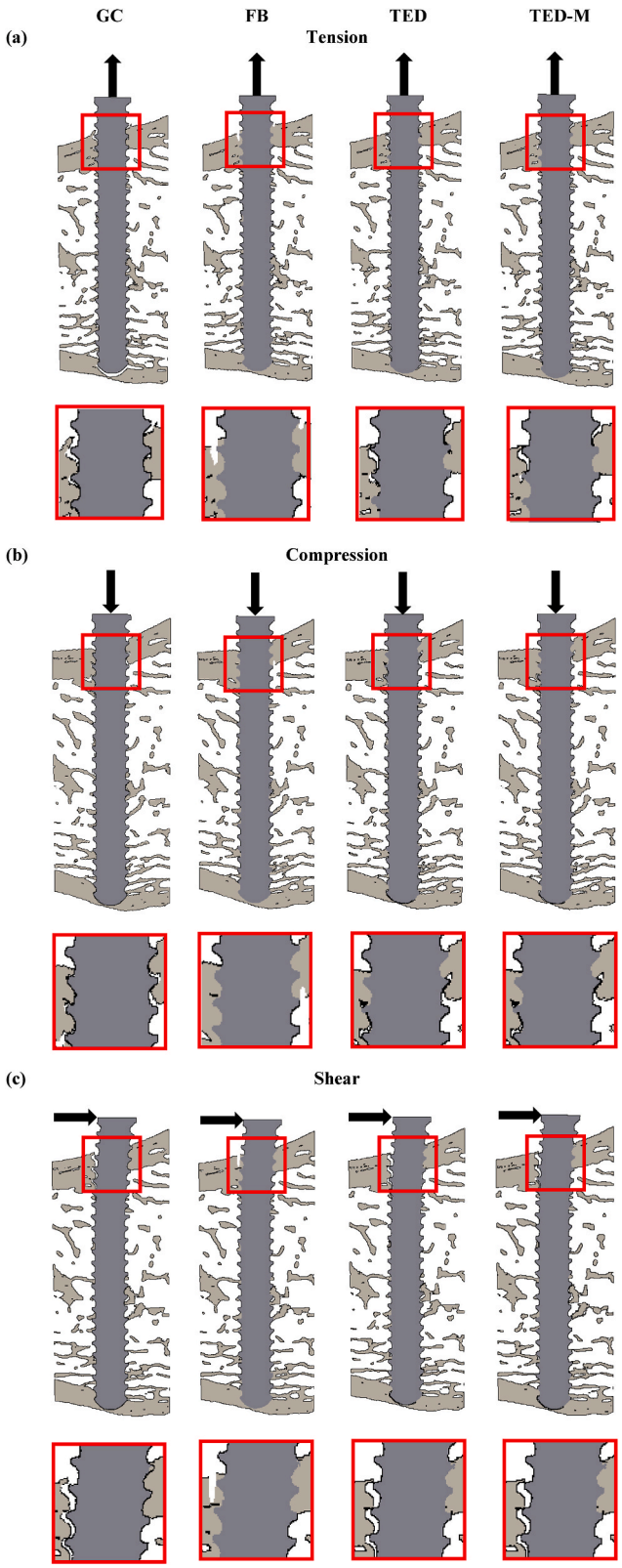

Fig. 2. Deformations at maximum force (scaling factor: 5) of one representative specimen (HD_100) with the general contact interface (GC), the fully-bonded interface (FB), the tensionally-strained element deletion interface (TED) and the modified tensionally-strained element deletion interface (TED-M) in tension (a), compression (b) and shear (c). The first row displays the entire specimen, with a red square highlighting regions that are magnified in the second row. Note: general contact (GC), fully-bonded (FB), tensionally-strained element deletion (TED), modified tensionally-strained element deletion (TED-M).

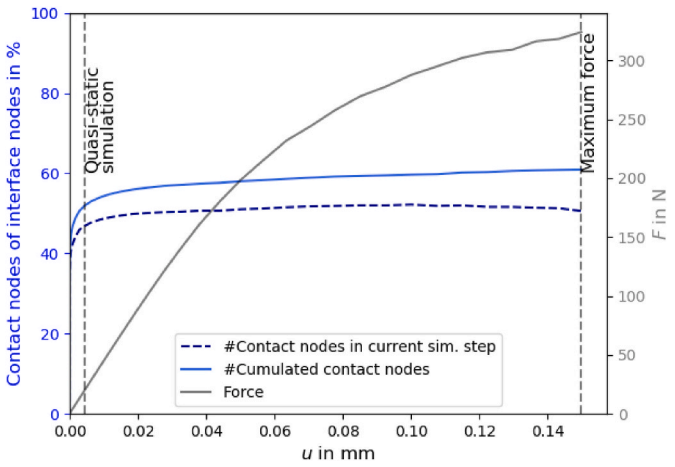

Fig. 3. Contact area analysis for one representative specimen (LD_50) in compression. Interface nodes belonged to elements that were included both in the bone and in the screw element set. Contact nodes were defined as interface nodes, when CPRESS >0. The number of contact nodes in each simulation step is shown over the whole simulation process until maximum force is reached. Furthermore, cumulated contact nodes are illustrated from the beginning of the simulation up to maximum force. They were measured by summing up all identified contact nodes and hence report changes in the contact area.

Table 2
Permanent contact nodes in % of all contact nodes that contributed to the contact area in at least one simulation step from quasi-static conditions to maximum force. Contact nodes were stated as permanent, if they were contact nodes in each reported simulation step from quasi-static conditions to maximum force.

	LD_50	LD_100	HD_50	HD_100
Permanent contact nodes in % of all contact nodes	**Tension**			
	64	55	62	64
	Compression			
	69	66	66	66
	Shear			
	43	42	55	54

Note: low-density specimen (LD), high-density specimen (HD), 50% screw insertion depth (50), 100% screw insertion depth (100).

intention to reduce simulation time while fully capturing the bone damage around the implant. The μCT image of a locking screw (Medartis A-5750; titanium alloy TiAl6V4), that was part of a distal radius fracture fixation system (A-5750; Medartis, Basel, Switzerland), was taken and resampled to 32.8 μm from Synek et al. (2023) (Skyscan 1173; Bruker, Bilerica, USA). The screw (outer diameter: 2.5 mm) was cut to different lengths and was virtually inserted into the center of the segmented bone images in two configurations: either the screw tip was aligned flushed with the outer surface of the dorsal cortex (hereon denoted as 100% insertion depth), or the screw was inserted to 50% of the volar-dorsal cortex distance (hereon denoted as 50% insertion depth). Hence, four different bone-screw specimens were created: a high-density specimen with 50% (HD_50) and 100% (HD_100) screw insertion depth and a low-density specimen with 50% (LD_50) and 100% (LD_100) screw insertion depth (see Fig. 1). All image processing steps were performed with Medtool 4.5 (Dr. Pahr Ingenieurs e.U., Pfaffstätten, Austria).

2.2. Mesh, material and boundary conditions

Based on the segmented bone images with the implanted screw, μFE models were generated. All voxels were directly converted into eight-noded hexahedral elements (C3D8R) with side length of 32.8 μm. Isotropic and homogeneous material properties were assigned. Bone was modelled using a damage-based material model recently introduced for

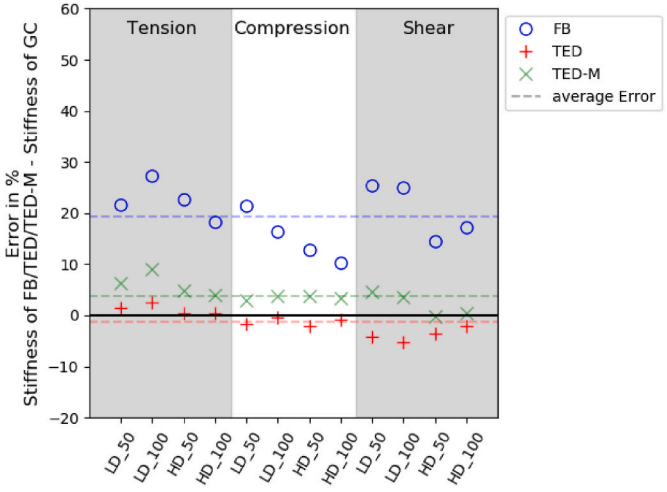

Fig. 5. Error of whole-construct stiffness results of FB, TED and TED-M interface simulations in comparison to reference simulation with interface GC in %. Note: low-density specimen (LD), high-density specimen (HD), 50% screw insertion depth (50), 100% screw insertion depth (100).

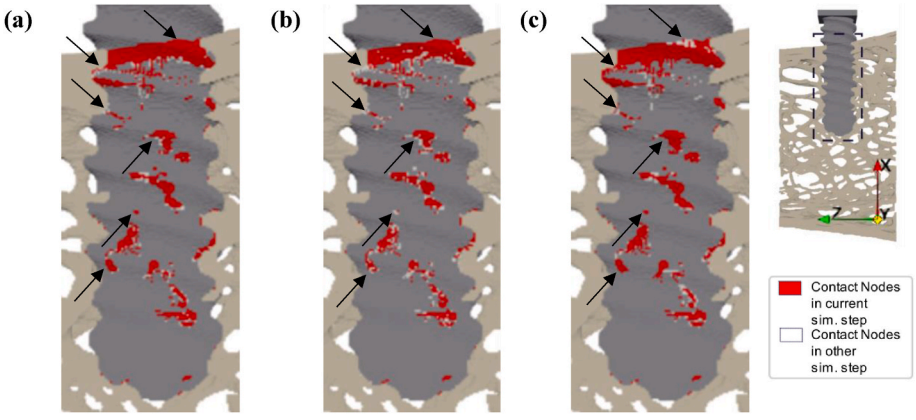

Fig. 4. Contact nodes for one representative specimen (LD_50) in compression at the start of the quasi-static simulation (a), in the middle of the simulation (b) and at maximum force (c). Interface nodes were defined as contact nodes, if CPRESS >0. Contact nodes, that contributed to the contact area in the current simulation step, were marked red while those, that were contact nodes in any other simulation step from quasi-static regime to maximum force, were marked white. The arrows point at regions which did not contribute to the contact area in all presented simulation steps, indicating a change in the contact area over the simulation time.

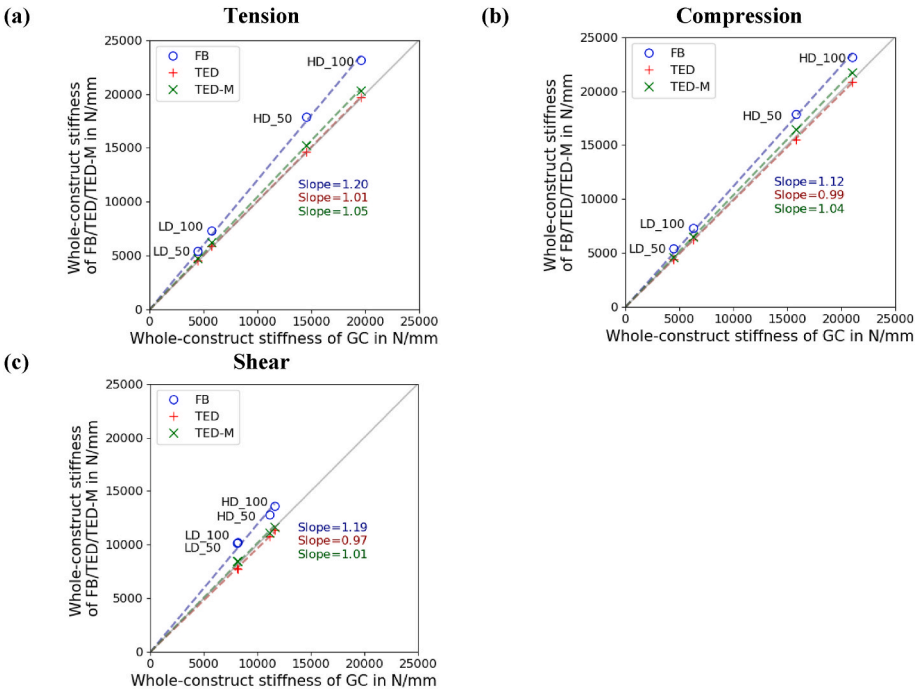

Fig. 6. Comparison of whole-construct stiffness results of FB, TED and TED-M interface simulations to stiffness of GC interface for all specimens in tension (a), compression (b) and shear (c).
Note: low-density specimen (LD), high-density specimen (HD), 50% screw insertion depth (50), 100% screw insertion depth (100).

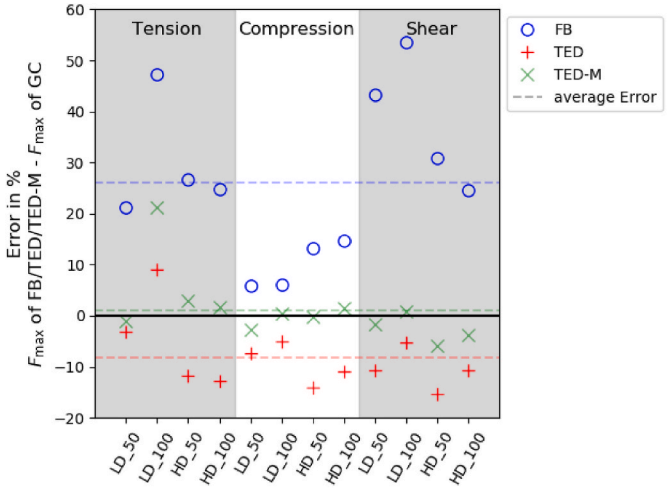

Fig. 7. Error of maximum force results of FB, TED and TED-M interface simulations in comparison to reference simulation with interface GC in %.
Note: low-density specimen (LD), high-density specimen (HD), 50% screw insertion depth (50), 100% screw insertion depth (100).

efficient large-scale nonlinear μFE analysis (Stipsitz et al., 2020). The material model was implemented as a user material (VUMAT) in Abaqus (Abaqus, 2022 Dassault Systems, Vélizy-Villacoublay, France) and included a linear-elastic region ($E_0 = 10$ GPa and a Poisson's ratio of $\nu = 0.3$), a damaged region with hardening (hardening modulus $E_H = 0.05\ E_0$) and a failure region. In the damaged region, material degradation was expressed via local stiffness reduction based on the observed damage. The yield criterion distinguished between tension and compression behavior (damage onset strain in tension $\varepsilon_0^+ = 0.0068$; damage onset strain in compression $\varepsilon_0^- = 0.0089$) and was modelled using an isotropic, quadric damage onset surface (shape parameter $\zeta_0 = 0.3$) (Stipsitz et al., 2020, 2021). Element deletion was enabled and elements that exceeded the critical damage D_c ($D_c = 0.915$) (Stipsitz et al., 2020, 2021) were deleted. The titanium alloy screw was modelled using linear-elastic material properties with an elastic modulus of $E = 115$ GPa and a Poisson's ratio of $\nu = 0.3$ (Synek et al., 2023).

The bone was fixed at the outer surfaces, except for the volar and dorsal surface (see Fig. 1). At the screw top, a displacement of 0.2 mm was applied in loading direction, while the movement in other directions was constrained. Three load cases were simulated. In tension and compression, the displacement was applied in volar/dorsal direction. For the shear load case, the screw was displaced in distal direction.

The models were generated using Medtool 4.5 and had an element number between five and ten million.

2.3. Interface modelling

Four different interface models were applied: general contact (GC), considered as the gold-standard and reference interface model; fully-bonded (FB), assuming bonding at the bone-screw interface; tensionally-strained element deletion (TED), as proposed by Steiner et al. (2017) and a novel modification of TED (TED-M), derived from the findings of the contact area investigation (see section 3.1). For the general contact interface, hard contact with a friction coefficient of 0.7 (Ovesy et al., 2019, 2022) was selected and self-contact was excluded for the screw material. With the element deletion technique activated, all contact surfaces were updated in every iteration in order to account for potential interface changes. TED is an interface model that represents contact in a simplified way (Steiner et al., 2017) (see Appendix A for a detailed explanation). Before the actual simulation, a single preliminary simulation ("pre-simulation") with the fully-bonded interface is conducted and evaluated in the linear-elastic region. Interface elements experiencing positive volumetric strain are identified as being strained in tension and are subsequently removed, under the assumption that no tensile stresses can be transferred at the contact interface. Conversely, interface elements undergoing negative volumetric strain are considered to be strained in compression and are retained in the interface, under the assumption that they contribute to the stress transfer between bone and

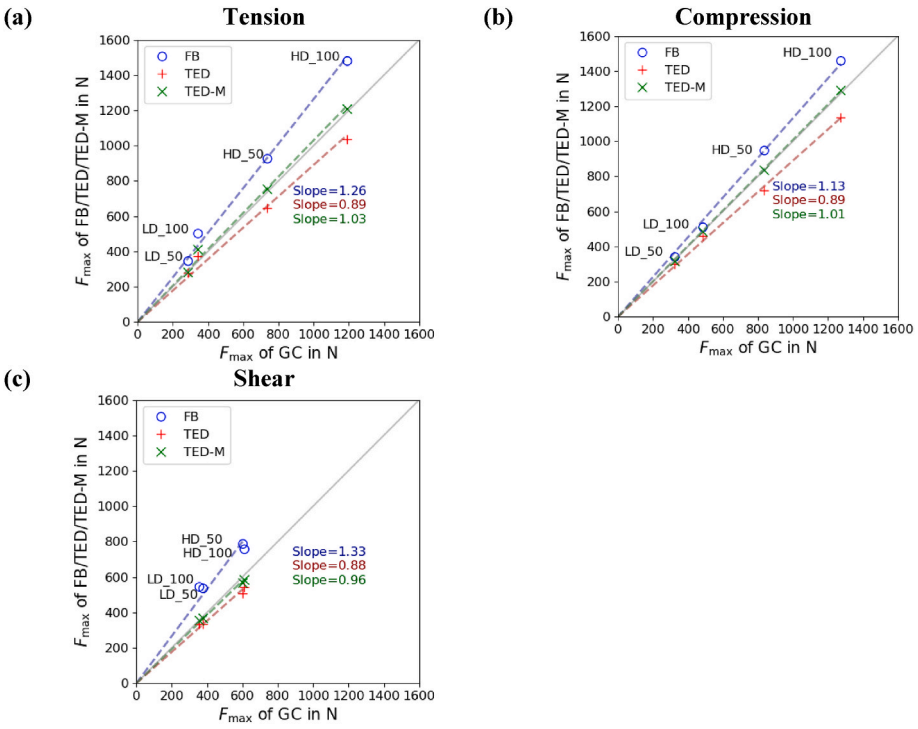

Fig. 8. Comparison of maximum force results of FB, TED and TED-M interface simulations to maximum force of GC interface for all specimens in tension (a), compression (b) and shear (c).
Note: low-density specimen (LD), high-density specimen (HD), 50% screw insertion depth (50), 100% screw insertion depth (100).

screw. After the removal of disconnected elements resulting from the deletion process, the final nonlinear simulation with the updated interface is performed. TED-M (see Appendix A for details) is a novel approach similar to TED, derived from the insights gained in section 3.1, which revealed a notable change in the contact area throughout the simulation process. TED may not fully capture these contact interface dynamics, as it relies on a single "pre-simulation". TED-M slightly increases the contact area of TED, in an effort to better capture the interface elements that get into contact throughout the entire simulation up to maximum force. It uses the contact interface detected with TED as starting point, but reincludes those interface elements with positive volumetric strain into the contact interface that share at least one node with the interface elements with negative volumetric strain. This approach derives from observations that contact area changes mainly involve neighboring interface elements (see section 3.1).

2.4. Simulation

All models were solved with Abaqus Explicit (Abaqus, 2022 Dassault Systems) using 29 cores on a dual AMD EPYX 7452 server with 512 GB RAM.

In order to minimize computational costs, a simulation time of t = 0.0005s was chosen, with results assessed at intervals of 1e-05s. Furthermore, a smooth loading amplitude was applied and bulk viscosity was assigned using the default parameters of Abaqus Explicit. The simulation ensured quasi-static behavior by confirming that kinetic energy did not exceed 5% of internal energy, except for the initial phase (Akhlaghi et al., 2023). Consequently, this initial phase was excluded from the results, with evaluations of all simulations (and "pre--simulations") starting once quasi-static conditions were established.

Additional simulations were performed to ensure that variations of voxel size (32.8 μm and 72 μm) and specimen size (side length of 7.5 mm and 9 mm) did not influence the main study outcomes (see Appendix B).

2.5. Reference model evaluation and contact area analysis

The contact area was examined using the contact output variable CPRESS in the simulations with the GC interface. CPRESS is evaluated at the element nodes and denotes the magnitude of the net contact normal force per unit area. An element was classified as interface element if it contained at least one interface node. A node was called an interface node, if its coordinates were included both in the bone and in the screw element set. An interface node was defined as contact node, when CPRESS >0. Contact nodes were categorized as permanent, if they contributed to the contact area in all simulation steps, while temporary contact nodes contributed to the contact area in at least one simulation step. The number of interface nodes, contributing to contact, was analyzed at each simulation step to estimate the size of the contact area. Furthermore, changes in the contact area over the simulation time were tracked by measuring the cumulative number of interface nodes contributing to the contact area in at least one simulation step. The contact area analysis only considered the parts of the simulation where quasi-static conditions (kinetic energy $\leq$5% of internal energy) were ensured up to the point of reaching maximum force.

2.6. Comparison of interfaces and contact area analysis

Simulations with the interfaces FB, TED and TED-M were compared to the reference interface model GC by analyzing deformations, whole-construct stiffness, maximum force and damage distribution within the bone. Deformation plots were generated at maximum force and analyzed in a qualitative manner. Whole-construct stiffness was measured by calculating the tangent slope of two prior defined displacement steps that lay in the quasi-static and elastic regime. Maximum force was defined as the peak force, followed by a force decrease of at least 10N. Linear regressions were performed for whole-construct stiffness and maximum force for each loading case individually. The regression line was constrained to pass through the origin to measure the average error of each specific interface method compared to

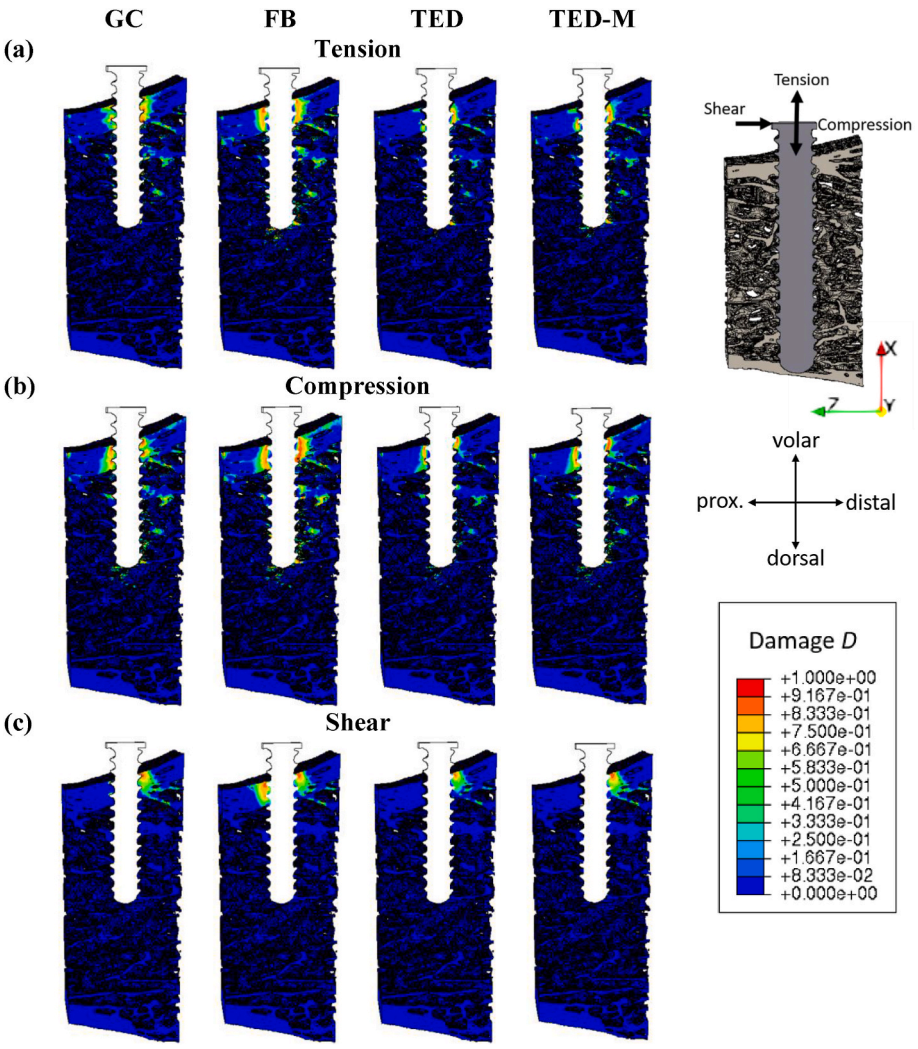

Fig. 9. Damage distribution at maximum force for the high-density specimen with screw insertion depth of 50% for all loading cases tension (a), compression (b), and shear (c).

the GC interface. Additionally, relative errors of all simulations in comparison to the simulation with the GC interface were computed. Damage distributions were evaluated, visualized and compared at maximum force. An element was considered as damaged if damage $D > 0$.

All statistical evaluations were performed with Python 3.8 (https://www.python.org/) and the included library SciPy (Virtanen et al., 2020). All figures showing the distribution of damage were created using Paraview (https://www.paraview.org/).

3. Results

3.1. Reference model evaluation and contact area analysis

Qualitative analysis of the deformed specimens at maximum force revealed that the general contact interface caused an opening of the bone-screw interface at the dorsal and volar cortex in the tension load case (see Fig. 2(a) GC). In the compression load case, bone-screw interface openings were harder to detect but could be observed especially at the volar cortex (see Fig. 2(b) GC). Similarly, in the shear case, an interface opening was detected at the volar cortex on the proximal side of the screw (see Fig. 2(c) GC).

At the starting point of the quasi-static regime, contact area analysis showed that between 38% and 48% of interface nodes were recognized as contact nodes for all specimens and loading cases (see Fig. 3 and supplementary material). As the simulation progressed, the number of contact nodes increased between 3% and 12% so that on average 52% of interface nodes contributed to the contact area. Then, the contact area stayed rather constant until a slight drop between 1% and 6% was found just before reaching maximum force.

The cumulative number of identified contact nodes ranged between 42% and 50% for all specimens and loading cases at the beginning of the quasi-static regime (see Fig. 3 and supplementary material). Subsequently, it exhibited a rapid increase followed by a slower ascent until it reached final values ranging between 52% and 72% for all specimens.

The number of permanent contact nodes ranged between 42% and 69% for all specimens and loading cases (see Table 2). The lowest constancy of contact area was observed in the shear case, the highest in the compression load case. The change in contact area over the simulation time is also shown in Fig. 4. Qualitative analysis revealed that the temporary contact nodes were mostly located around the permanent contact nodes.

3.2. Deformation

The differences in the deformation between the interface models were particularly evident in the dorsal and volar cortex (see Fig. 2(a–c)). At maximum force in tension, all simplified contact models (FB, TED,

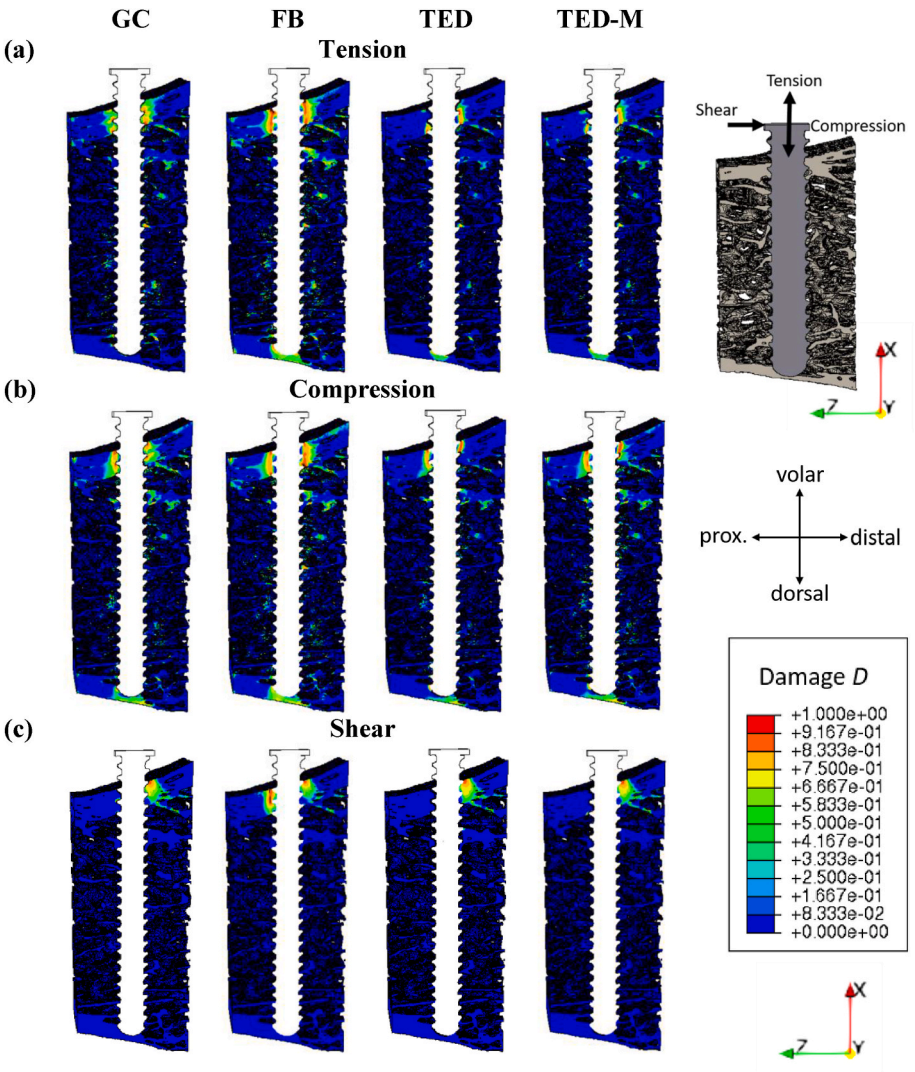

Fig. 10. Damage distribution at maximum force for the high-density specimen with screw insertion depth of 100% for all loading cases tension (a), compression (b) and shear (c).
Note: general contact (GC), fully-bonded (FB), tensionally-strained element deletion (TED), modified tensionally-strained element deletion (TED-M).

TED-M) stayed completely (see Fig. 2(a) FB) or mainly (Fig. 2(a) TED, TED-M) bonded at the dorsal cortex. At the volar cortex, the FB interface stayed completely bonded, while TED and TED-M mostly replicated the interface opening of the general contact interface. In the compression and shear load case, interface openings were hardly detectable at the dorsal cortex. At the volar cortex, the FB interface stayed bonded while TED and TED-M again replicated the GC interface (see Fig. 2(b) and (c) FB, TED, TED-M).

3.3. Whole-construct stiffness

The FB interface simulations of all specimens overestimated the whole-construct stiffness between 10% and 27% with an average error of 19% in comparison to the GC interface (see Fig. 5). The overestimation was lowest in compression (12%) and highest in tension (20%) (see Fig. 6).

TED achieved the most accurate replication of whole-construct stiffness results among all interface models, with an average underestimation error of only 1%. The error ranged between −5% and 2% over all specimens, meaning that for some the whole-construct stiffness was underestimated, while it was overestimated for others (see Fig. 5). Underestimation was highest in the shear case (3%), reduced in compression (1%) and turned into an overestimation in the tension case (1%) (see Fig. 6).

TED-M interface simulations demonstrated enhanced whole-construct stiffness replication compared to the FB interface, with an average error of 4% across all specimens and loading cases (see Fig. 5). The overestimation in tension (5%) and compression (4%) was higher than in shear (1%) (see Fig. 6).

3.4. Maximum force

Simulations with the FB interface led to an overestimation of maximum force for all specimens and all loading cases with an average error of 26% in comparison to the GC interface. Especially in the tension and shear loading cases high errors between 21% and 54% were found. With an average error of 13%, errors were much lower in the compression case (see Fig. 7).

TED was able to reduce the maximum force error in comparison the FB interface, but turned the maximum force overestimation into an underestimation. All specimens and all loading cases, except for the low-density specimen with 100% screw insertion depth (LD_100) in tension, showed an underestimation of maximum force ranging between 5% and 15% with the TED interface (see Fig. 7).

TED-M improved the maximum force replication in comparison to TED and FB and reduced the average error of all specimens and loading

cases to 1%. Except for specimen LD_100 in tension, the maximum force error was by 6% at most. For specimen LD_100 a large overestimation of 21% was observed (see Fig. 7). Separation of the loading cases showed that the shear loading case leads to an underestimation of 4% on average, while tension and compression overestimated the maximum force for up to 3% on average (see Fig. 8).

3.5. Damage distributions

Qualitative analysis of damage showed that the simulation with the FB interface resulted in a different damage pattern in comparison to the simulation with GC for all loading cases and for all specimens (see Figs. 9 and 10). The amount and the magnitude of damage were higher with the FB interface. Especially the shear load case showed that FB was not able to qualitatively replicate the damage of the GC interface simulation (see Figs. 9(c) and 10(c)). The volar cortex was damaged on both sides of the screw, which was not the case with the GC interface.

TED and TED-M both led to damage patterns that resembled GC better than FB. TED-M showed slightly more damaged regions and also the magnitude of damage was higher. Therefore, TED-M replicated the damage pattern of GC slightly better than TED. The improved damage replication in comparison to FB can be observed in the shear case where the damage was reduced to the distal side of the volar cortex similar to the result of GC. However, the damage distribution still showed differences to GC, particularly in the tension simulation of the high-density specimen with 100% screw insertion depth (HD_100) (see Fig. 10(a)). Damage at the dorsal cortex was observed in both TED and TED-M, despite its absence in GC.

4. Discussion

This numerical study aimed to compare different simplified interface approaches regarding deformations, whole-construct stiffness, maximum force, and damage using materially-nonlinear μFE simulations of bone-screw systems. General contact in Abaqus Explicit was defined as gold-standard and reference model. The first objective was to evaluate the impact of physical contact modelling, achieved through a comparison between the fully-bonded approach and the general contact model. All specimens and loading cases showed whole-construct stiffness and maximum force overestimations, as well as differing damage patterns. However, the average error of 19% for whole-construct stiffness and 26% for maximum force of the fully-bonded approach may be acceptable for many applications. The computationally efficient "element deletion" models TED, as presented by Steiner et al. (2017), and the novel TED-M model, both enhanced the predictions of the fully-bonded approach and hence enabled efficient and even more accurate predictions of deformations, whole-construct stiffness, maximum force and especially damage patterns.

While the maximum force results of the general contact interface model were generally in line with the μFE results reported in literature (Ovesy et al., 2022; Panagiotopoulou et al., 2021), the whole-construct stiffness results reported by Ovesy et al. (2019) were lower than the values of this study (max. 4 kN/mm vs. max. 21 kN/mm). This mismatch can be explained by several factors, e.g. Ovesy et al. (2019) used trabecular bone specimens and inserted a dental implant, while in this study locking screws were implanted into specimens consisting of trabecular bone with cortex.

The whole-construct stiffness predicted with the fully-bonded approach matched the results of Steiner et al. (2017) and Wirth et al. (2010). When comparing the whole-construct stiffness results of the fully-bonded model to the general contact model, whole-construct stiffness overestimations up to 27% were reported in this study, while Steiner et al. (2017) and Wirth et al. (2010) measured whole-construct stiffness overestimations of more than 300% on average when comparing their results to experiments. This mismatch likely results from the peri-implant bone damage occurring from the implantation process, which is included in experiments, but not modelled in this study. Peri-implant bone damage due to screw insertion has already been proven to cause whole-construct stiffness reduction (Lee and Baek, 2010; Steiner et al., 2016; Wang et al., 2012), hence explaining the large overestimations reported by Steiner et al. (2017) and Wirth et al. (2010). These results indicate that physical contact modelling only plays a minor role for predicting whole-construct stiffness in comparison to the reduced mechanical competence caused by peri-implant bone damage.

The relevance of physical contact modelling differs between the load cases. The lowest average errors in whole-construct stiffness and especially in maximum force were measured in the compression load case, where all interface elements at the screw tip retain the screw movement regardless of whether they are bonded or in contact. In contrast, in the fully-bonded tension and shear simulations, the interface elements are bonded to the screw and hence oppose the tension and shear movement, which is not the case in the general contact simulation. In conclusion, physical contact modelling showed importance, as we saw overestimation errors and different damage pattern patterns for all specimens and loading cases. Nonetheless, the overestimations of whole-construct stiffness and maximum force may be acceptable for many applications. For instance, the fully-bonded approach may be appropriate for predicting whole-construct stiffness in the presence of peri-implant bone-damage, considering that peri-implant bone damage likely exerts a larger influence on the results than interface modelling. However, fully-bonded models should be avoided when the aim is to investigate damage patterns.

Although both TED and TED-M enhanced the predictive accuracy of deformations, whole-construct stiffness, maximum force and damage patterns in comparison to the fully-bonded approach, they exhibited performance differences. The interface model TED discriminates between interface elements strained in tension and compression only in a single simulation step in the elastic regime and hence fails to account for the occurring contact area changes. This seems to be sufficient to replicate whole-construct stiffness (average error of 1%) but not maximum force (average error of 8%). Consequently, TED was enhanced to TED-M by expanding the contact area to account for the contact area changes. Since contact analysis revealed that non-permanent contact nodes predominantly surrounded permanent ones, the contact area increase was achieved by including neighboring interface elements of contact elements to the contact area. TED-M was able to improve the force predictions to an error of 1% on average, but led to slight whole-construct stiffness overestimations (average error of 4%). Nevertheless, neither TED not TED-M could perfectly replicate the general contact model, as evidenced in the damage pattern of the tension load case of the specimens with 100% screw insertion depth. Both TED and TED-M did not delete all elements below the screw tip inducing an incorrect damage prediction. This incorrect damage replication later resulted in an overestimation of maximum force, particularly notable in the low-density sample (LD_100), where the sparse trabecular bone only minimally contributes to the maximum force result. These results indicate that in order to replicate the general contact model more accurately, an interface model that includes a change in the contact elements throughout the simulation is required. Nonetheless, increasing the complexity of the interface model by including repeated contact element deletion comes with the drawback of reduced model efficiency.

The study faces several limitations. Firstly, the study was conducted solely numerical and specified general contact as gold standard. Although the general contact algorithm still remains to be validated to clarify its capability of physical contact replication, its application is common practice in the majority of research studies that implement bone-screw contact (Akhlaghi et al., 2023; Ovesy et al., 2019). The virtual screw insertion process did not consider peri-implant bone damage which might have a large effect on the interface and was found to have high influence at least on the whole-construct stiffness results (Steiner et al., 2017). Nonetheless, we decided to isolate the contact effects in order to avoid the overlapping of interface modelling and

peri-implant damage influences in the results. Furthermore, all μFE models were based on hexahedral voxel elements, which might not be able to perfectly display the bone and screw geometry and hence the contact surfaces. Despite this limitation being inherent to all μFE simulations, the used voxel size was comparable or even smaller than in many similar studies (Ovesy et al., 2019, 2022; Panagiotopoulou et al., 2021). The analyses were restricted to small bone regions in order to achieve feasible solving times for the nonlinear simulations. It was ensured that the cropped regions were large enough the capture the effects of the compared interface models (Ovesy et al., 2019, 2022). Next, the study results are based on the used nonlinear material model, the selected material parameters and resolution proposed by Stipsitz et al. (2020) and a commonly used friction coefficient taken from Ovesy et al. (2019). Although the main study outcomes could be replicated for lower resolutions (see Appendix B), the influence of other parameters still needs to be investigated. Lastly, the study was limited to a single screw, two bone specimens with varying densities and two insertion depths.

5. Conclusion

This study compared three different simplified interface modelling approaches in materially nonlinear μFE simulations of bone-screw systems regarding deformations, whole-construct stiffness, maximum force and damage distribution using general contact as gold-standard. Overestimations in whole-construct stiffness and maximum force, along with differing damage patterns between the fully-bonded and general contact interfaces, showed the relevance of physical contact modelling. However, the errors of the fully-bonded approach may be acceptable for many applications, particularly if the damage pattern is of minor relevance. The simplified interface models TED and TED-M effectively reduced errors and improved damage pattern predictions, with TED outperforming in whole-construct stiffness prediction and TED-M exhibiting the lowest errors in maximum force. These interface models offer computational efficiency and straightforward implementation in μFE solvers like ParOSol-NL. Consequently, this research study serves as an initial step towards enabling simulations of complete bone-screw implant systems with enhanced accuracy and efficiency beyond the current capabilities.

CRediT authorship contribution statement

Pia Stefanek: Writing – original draft, Visualization, Project administration, Methodology, Investigation. **Dieter H. Pahr:** Writing – review & editing, Supervision, Resources, Conceptualization. **Alexander Synek:** Writing – review & editing, Supervision, Methodology, Investigation, Conceptualization.

Declaration of generative AI and AI-assisted technologies in the writing process

During the preparation of this work the authors used ChatGPT in order to improve readability and language. After using this tool, the authors reviewed and edited the content as needed and take full responsibility for the content of the publication.

Declaration of competing interest

The authors declare the following financial interests/personal relationships which may be considered as potential competing interests:

DP is CEO of Dr. Pahr Ingenieurs e.U. which develops and distributes the software Medtool. PS and AS have no conflicts of interest to declare.

Data availability

Data will be made available on request.

Acknowledgements

The authors acknowledge TU Wien Bibliothek for financial support through its Open Access Funding Programme.

Appendix A

Both, TED and TED-M are “element deletion” interface models that represent contact in a simplified way.

In a first step, TED performs a single preliminary simulation (“pre-simulation”) with the fully-bonded interface (see Fig. A1(a) Step 1). Volumetric strain is evaluated in the linear-elastic regime and interface elements are discriminated based on their volumetric strain value (see Fig. A1(a) Step 2). Interface elements, that experience positive volumetric strain, are identified as being strained in tension, while interface elements, undergoing negative volumetric strain, are considered to be strained in compression. Under the assumption that only elements strained in compression contribute to the stress transfer between bone and screw, interface elements, strained in tension, are deleted (see Fig. A1(a) Step 3). Only interface elements strained in compression remain in the updated interface. After the removal of newly appeared disconnected elements resulting from the deletion process, the simulation is performed again with the updated interface.

The first two steps of TED-M are equivalent to TED. A single “pre-simulation” is conducted and the interface elements are discriminated based on their volumetric strain value (see Fig. A1(b) Step 1 and 2). Conversely to TED, not all elements that were identified to be strained in tension get deleted, but TED-M reincludes some of them back into the contact interface. In step 3, TED-M finds interface elements identified to be strained into tension that have a shared node with interface elements considered to be strained in compression. Those so-called neighbor-elements of the interface elements strained in compression are reincluded into the updated interface. Only interface elements, that are strained in tension and have no shared node with interface elements strained in compression, get deleted (see Fig. A1(b) Step 4). Similar to TED, newly appeared disconnected elements, resulting from the deletion process, get deleted and the simulation with the updated interface is performed again.

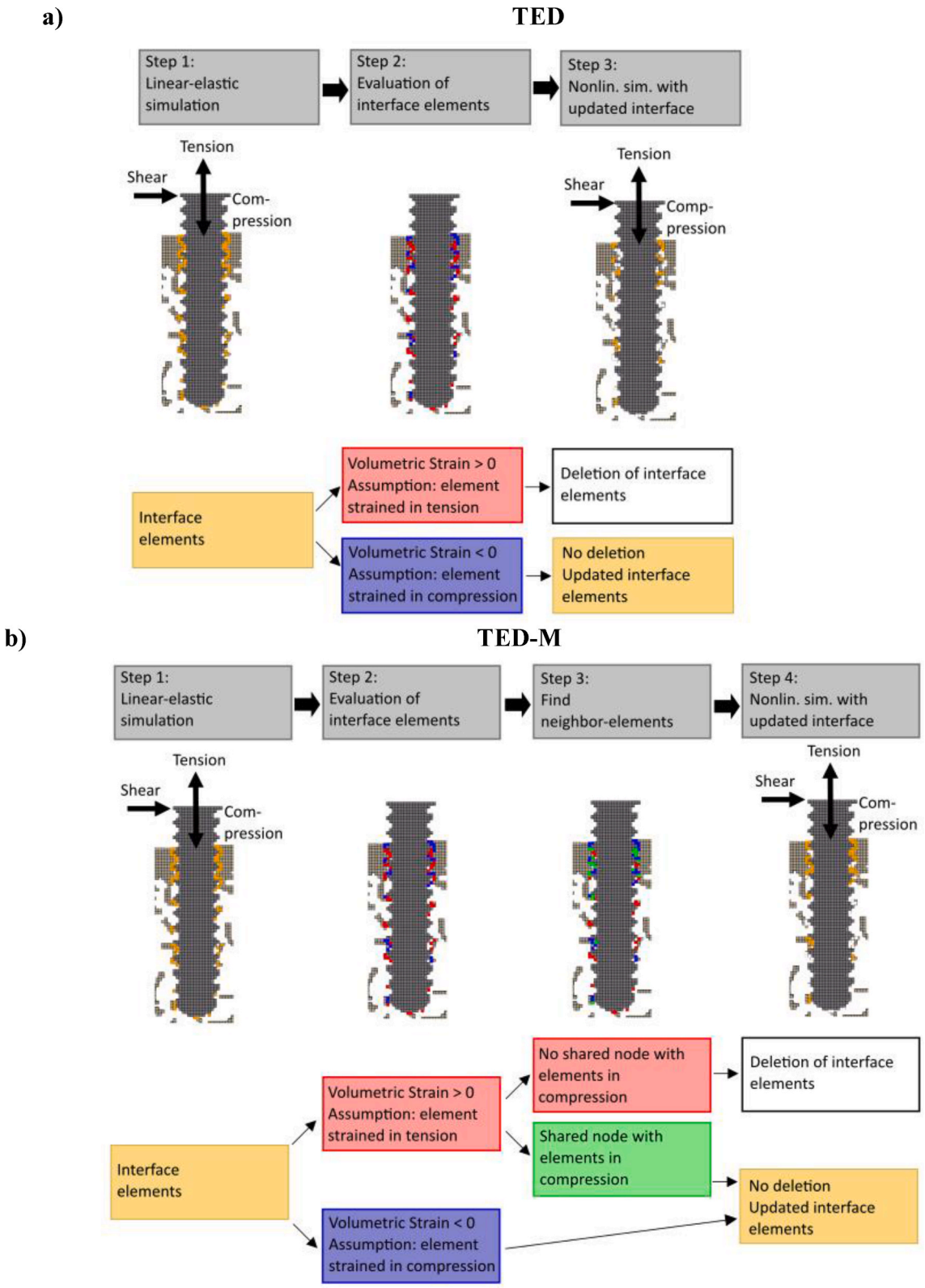

Fig. A.1. Workflow of TED (a) and TED-M (b). This figure shows the interface models with lower resolution in order to schematically illustrate the differences at the interface. TED deletes interface elements based on their volumetric strain value (volumetric strain >0 → deletion) in a linear-elastic preliminary simulation and performs the actual simulation with the updated interface. TED-M increases the contact area of TED by reincluding neighboring interface elements of the updated interface.

Appendix B

The influence of the voxel size (32.8 μm and 72 μm) on the main outcomes of this study was investigated in tension for the low-density and high-

density specimen with 50% screw insertion depth (LD_50 and HD_50) (see Fig. B1). TED was best in replicating whole-construct stiffness (see Fig. B1 (a)), while TED-M showed lowest errors in maximum force (see Fig. B1(b)) for all resolutions and sample sizes. The influence of the specimen size (7.5 mm and 9 mm) was explored in tension on the high-density specimen with 50% screw insertion depth (HD_50) (see Fig. B2). Again, TED exhibited lowest errors in whole-construct stiffness replication (see Fig. B2(a)), while TED-M mostly enhanced the maximum force predictions (see Fig. B2(b)). These results suggest that both voxel and specimen size variations only had negligible influence the main study outcomes.

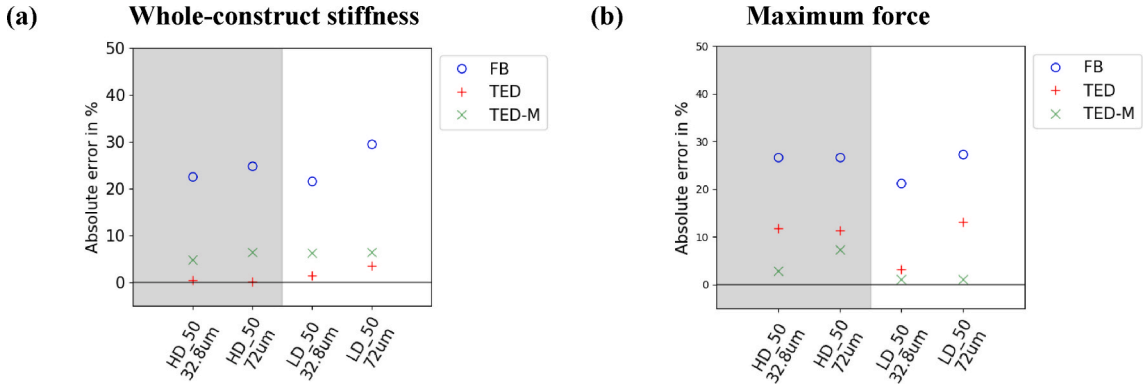

Fig. B.1. Absolute error in whole-construct stiffness (a) and maximum force (b) when comparing the simplified interface models fully-bonded (FB), tensionally strained element deletion (TED) and modified TED (TED-M) to the general contact model (GC) for two different resolutions (32.8 μm and 72 μm) for the high-density specimen with 50% screw insertion depth (HD_50) and the low-density specimen with 50% screw insertion depth (LD_50) in tension.

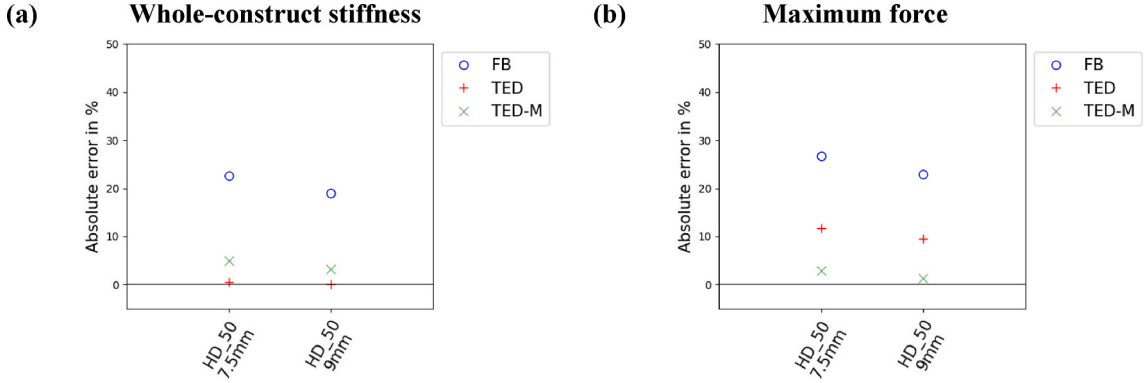

Fig. B.2. Absolute error in whole-construct stiffness (a) and maximum force (b) when comparing the simplified interface models fully-bonded (FB), tensionally strained element deletion (TED) and modified TED (TED-M) to the general contact model (GC) for two different sample sizes (7.5mmnd 9 mm) for the high-density specimen with 50% screw insertion depth (HD_50) in tension.

Appendix C. Supplementary data

Supplementary data to this article can be found online at https://doi.org/10.1016/j.jmbbm.2024.106634.

References

Akhlaghi, P., Khorshidparast, S., Rouhi, G., 2023. Investigation on primary stability of dental implants through considering peri-implant bone damage, caused by small and large deformations: a validated non-linear micro finite element study. J. Mech. Behav. Biomed. Mater. 146, 106062 https://doi.org/10.1016/j.jmbbm.2023.106062.

Flaig, C., Arbenz, P., 2012. A highly scalable matrix-free multigrid solver for μFE analysis based on a pointer-less octree. Large-Scale Sci. Comput. 498–506.

Hosseini, H.S., Dünki, A., Fabech, J., Stauber, M., Vilayphiou, N., Pahr, D., Pretterklieber, M., Wandel, J., van Rietbergen, B., Zysset, P.K., 2017. Fast estimation of Colles' fracture load of the distal section of the radius by homogenized finite element analysis based on HR-pQCT. Bone 97, 65–75. https://doi.org/10.1016/j.bone.2017.01.003.

Lee, N.K., Baek, S.H., 2010. Effects of the diameter and shape of orthodontic mini-implants on microdamage to the cortical bone. Am. J. Orthod. Dentofacial Orthop. 138 (1), 8.e1–8.e8. https://doi.org/10.1016/j.ajodo.2010.02.019.

Marcián, P., Borák, L., Zikmund, T., Horáčková, L., Kaiser, J., Joukal, M., Wolff, J., 2021. On the limits of finite element models created from (micro)CT datasets and used in studies of bone-implant-related biomechanical problems. J. Mech. Behav. Biomed. Mater. 117 https://doi.org/10.1016/j.jmbbm.2021.104393.

Ovesy, M., Indermaur, M., Zysset, P.K., 2019. Prediction of insertion torque and stiffness of a dental implant in bovine trabecular bone using explicit micro-finite element analysis. J. Mech. Behav. Biomed. Mater. 98, 301–310. https://doi.org/10.1016/j.jmbbm.2019.06.024.

Ovesy, M., Silva-Henao, J.D., Fletcher, J.W.A., Gueorguiev, B., Zysset, P.K., Varga, P., 2022. Non-linear explicit micro-FE models accurately predict axial pull-out force of cortical screws in human tibial cortical bone. J. Mech. Behav. Biomed. Mater. 126 https://doi.org/10.1016/j.jmbbm.2021.105002.

Panagiotopoulou, V.C., Ovesy, M., Gueorguiev, B., Richards, R.G., Zysset, P., Varga, P., 2021. Experimental and numerical investigation of secondary screw perforation in the human proximal humerus. J. Mech. Behav. Biomed. Mater. 116 https://doi.org/10.1016/j.jmbbm.2021.104344.

Steiner, J.A., Christen, P., Affentranger, R., Ferguson, S.J., van Lenthe, G.H., 2017. A novel in silico method to quantify primary stability of screws in trabecular bone. J. Orthop. Res. 35 (11), 2415–2424. https://doi.org/10.1002/jor.23551.

Steiner, J.A., Ferguson, S.J., van Lenthe, G.H., 2016. Screw insertion in trabecular bone causes peri-implant bone damage. Med. Eng. Phys. 38 (4), 417–422. https://doi.org/10.1016/j.medengphy.2016.01.006.

Stipsitz, M., Pahr, D.H., 2018. *AN efficient solver for LARGE-SCALE simulations of VOXEL-BASED structures using A nonlinear damage material model* (issue 7). https://www.ilsb.tuwien.ac.at.

Stipsitz, M., Zysset, P.K., Pahr, D.H., 2020. Efficient materially nonlinear μFE solver for simulations of trabecular bone failure. Biomech. Model. Mechanobiol. 19 (3), 861–874. https://doi.org/10.1007/s10237-019-01254-x.

Stipsitz, M., Zysset, P.K., Pahr, D.H., 2021. Prediction of the inelastic behaviour of radius segments: damage-based nonlinear micro finite element simulation vs pistoia criterion. J. Biomech. 116 https://doi.org/10.1016/j.jbiomech.2020.110205.

Synek, A., Ortner, L., Pahr, D.H., 2023. Accuracy of osseointegrated screw-bone construct stiffness and peri-implant loading predicted by homogenized FE models relative to

micro-FE models. J. Mech. Behav. Biomed. Mater. 140 https://doi.org/10.1016/j.jmbbm.2023.105740.
Taylor, M., Prendergast, P.J., 2015. Four decades of finite element analysis of orthopaedic devices: where are we now and what are the opportunities? J. Biomech. 48 (5), 767–778. https://doi.org/10.1016/j.jbiomech.2014.12.019.
Taylor, R.L., 2014. FEAP - Finite Element Analysis Program. University of California, Berkeley. http://www.ce.berkeley/feap.
Torcasio, A., Zhang, X., Van Oosterwyck, H., Duyck, J., Van Lenthe, G.H., 2012. Use of micro-CT-based finite element analysis to accurately quantify peri-implant bone strains: a validation in rat tibiae. Biomech. Model. Mechanobiol. 11 (5), 743–750. https://doi.org/10.1007/s10237-011-0347-6.
Virtanen, P., Gommers, R., Oliphant, T.E., Haberland, M., 2020. SciPy 1.0: fundamental algorithms for scientific computing in Python. Nat. Methods 17 (3), 261–272.
Wang, L., Shao, J., Ye, T., Deng, L., Qiu, S., 2012. Three-dimensional morphology of microdamage in peri-screw bone: a scanning electron microscopy of methylmethacrylate cast replica. Microsc. Microanal. 18 (5), 1106–1111. https://doi.org/10.1017/S1431927612001286.
Wirth, A.J., Goldhahn, J., Flaig, C., Arbenz, P., Müller, R., Van Lenthe, G.H., 2011. Implant stability is affected by local bone microstructural quality. Bone 49 (3), 473–478. https://doi.org/10.1016/j.bone.2011.05.001.
Wirth, A.J., Mueller, T.L., Vereecken, W., Flaig, C., Arbenz, P., Müller, R., Van Lenthe, G. H., 2010. Mechanical competence of bone-implant systems can accurately be determined by image-based micro-finite element analyses. Arch. Appl. Mech. 80 (5), 513–525. https://doi.org/10.1007/s00419-009-0387-x.
Wirth, A.J., Müller, R., Harry van Lenthe, G., 2012. The discrete nature of trabecular bone microarchitecture affects implant stability. J. Biomech. 45 (6), 1060–1067. https://doi.org/10.1016/j.jbiomech.2011.12.024.